ENVIRONMENTAL RESEARCH
LETTERS

LETTER • OPEN ACCESS

Sustained methane emissions from China after 2012 despite declining coal production and rice-cultivated area

To cite this article: Jianxiong Sheng *et al* 2021 *Environ. Res. Lett.* **16** 104018

ENVIRONMENTAL RESEARCH
LETTERS

LETTER

Sustained methane emissions from China after 2012 despite declining coal production and rice-cultivated area

Jianxiong Sheng[1], **Rachel Tunnicliffe**[2,3], **Anita L Ganesan**[3], **Joannes D Maasakkers**[4], **Lu Shen**[5], **Ronald G Prinn**[1], **Shaojie Song**[5], **Yuzhong Zhang**[6,7], **Tia Scarpelli**[5], **A Anthony Bloom**[8], **Matthew Rigby**[2], **Alistair J Manning**[9], **Robert J Parker**[10,11], **Hartmut Boesch**[10,11], **Xin Lan**[12,13], **Bo Zhang**[14], **Minghao Zhuang**[15] and **Xi Lu**[16]

[1] Center for Global Change Science, Massachusetts Institute of Technology, Cambridge, MA, United States of America
[2] School of Chemistry, University of Bristol, Bristol, United Kingdom
[3] School of Geographical Sciences, University of Bristol, Bristol, United Kingdom
[4] SRON Netherlands Institute for Space Research, Utrecht, The Netherlands
[5] School of Engineering and Applied Science, Harvard University, Cambridge, MA, United States of America
[6] Key Laboratory of Coastal Environment and Resources of Zhejiang Province, School of Engineering, Westlake University, Hangzhou, Zhejiang, People's Republic of China
[7] Institute of Advanced Technology, Westlake Institute for Advanced Study, Hangzhou, Zhejiang, People's Republic of China
[8] Jet Propulsion Laboratory, California Institute of Technology, Pasadena, CA, United States of America
[9] Hadley Centre, Met Office, Exeter, United Kingdom
[10] National Centre for Earth Observation, University of Leicester, Leicester, United Kingdom
[11] Earth Observation Science, School of Physics and Astronomy, University of Leicester, Leicester, United Kingdom
[12] Global Monitoring Laboratory, National Oceanic and Atmospheric Administration, Boulder, CO, United States of America
[13] Cooperative Institute for Research in Environmental Sciences, University of Colorado, Boulder, CO, United States of America
[14] State Key Laboratory of Coal Resources and Safe Mining, China University of Mining & Technology (Beijing), Beijing, People's Republic of China
[15] College of Resources and Environmental Sciences, China Agricultural University, Beijing, People's Republic of China
[16] School of Environment, State Key Joint Laboratory of Environment Simulation and Pollution Control, Tsinghua University, Beijing, People's Republic of China

E-mail: shengj@mit.edu

Keywords: emissions, coal mining, methane, aquaculture, rice cultivation, china

Supplementary material for this article is available online

OPEN ACCESS

RECEIVED
25 June 2021

REVISED
2 September 2021

ACCEPTED FOR PUBLICATION
8 September 2021

PUBLISHED
27 September 2021

Abstract

China's anthropogenic methane emissions are the largest of any country in the world. A recent study using atmospheric observations suggested that recent policies aimed at reducing emissions of methane due to coal production in China after 2010 had been largely ineffective. Here, based on a longer observational record and an updated modelling approach, we find a statistically significant positive linear trend (0.36 ± 0.04 ($\pm 1\sigma$) Tg CH_4 yr^{-2}) in China's methane emissions for 2010–2017. This trend was slowing down at a statistically significant rate of -0.1 ± 0.04 Tg CH_4 yr^{-3}. We find that this decrease in growth rate can in part be attributed to a decline in China's coal production. However, coal mine methane emissions have not declined as rapidly as production, implying that there may be substantial fugitive emissions from abandoned coal mines that have previously been overlooked. We also find that emissions over rice-growing and aquaculture-farming regions show a positive trend (0.13 ± 0.05 Tg CH_4 yr^{-2} for 2010–2017) despite reports of shrinking rice paddy areas, implying potentially significant emissions from new aquaculture activities, which are thought to be primarily located on converted rice paddies.

1. Introduction

Methane is the second most important anthropogenic greenhouse gas after carbon dioxide and accounts for nearly 25% of radiative forcing since the pre-industrial era (Myhre *et al* 2014). It has been highlighted as an important target for meeting climate policies such as the Paris Agreement (Ganesan *et al* 2019). Global methane concentrations stabilized in the atmosphere from 1999 to 2006 but growth resumed in 2007 (Rigby *et al* 2008, Dlugokencky *et al* 2009) and still continues at some of the highest rates

in the recent measurement record (Nisbet *et al* 2019). The causes of these recent changes in the atmosphere remain controversial (Helmig *et al* 2016, Schaefer *et al* 2016, Rigby *et al* 2017, Turner *et al* 2017, 2019, Worden *et al* 2017, Saunois *et al* 2020, Zhao *et al* 2020).

China is the largest anthropogenic methane emitting country in the world according to United Nations Framework Convention on Climate Change (UNFCCC) reports (UNFCCC 2020). Coal mining, rice cultivation, ruminant livestock, and waste management are thought to account for about 90% of the country's total methane emissions (Chen *et al* 2013, Peng *et al* 2016, Janssens-Maenhout *et al* 2019, Sheng *et al* 2019). Previous inverse analyses (or 'top-down', atmospheric data-based estimates) of satellite and surface network observations suggested that China's annual emissions grew by $\sim$1 Tg CH_4 yr^{-1} from 2000 to 2010 (Bergamaschi *et al* 2013, Thompson *et al* 2015), and that this trend continued for 2010–2015 (Miller *et al* 2019), primarily attributed to increased emissions from coal mining. However, recent bottom-up inventory estimates using localized emission factors and information on coal production from China (Zhu *et al* 2017, Sheng *et al* 2019) show that China's coal mine methane (CMM) emissions have instead stabilized or decreased since 2012, with coal production declining by about 10% by 2017 from the peak levels in 2012/2013. There are also emerging sources such as abandoned coal mines and freshwater aquaculture (Yuan *et al* 2019, Gao *et al* 2020), which have not been assessed by previous inverse modeling studies.

Here we use eight years (2010–2017) of Greenhouse Gases Observing Satellite (GOSAT) column methane observations (Parker *et al* 2015) and high frequency data from the National Institute for Environmental Studies Japan (NIES) surface network at Cape Ochiishi and Hateruma in Japan (Tohjima *et al* 2014) to estimate methane emissions and trends in China through a regional Bayesian inverse analysis. Our regional inverse approach has the benefit over previous global studies (Maasakkers *et al* 2019, Miller *et al* 2019) because it estimates methane emissions at higher spatial resolution (crucial for accurate source attribution) and is independent of the large uncertainties in the main sink (Rigby *et al* 2017, Turner *et al* 2017), atmospheric oxidation by the hydroxyl radical. Source emission attribution often relies on knowledge of relative fractions of sectoral emissions within model grid cells. We use state-of-the-art bottom-up inventories as the prior for the inversion, which include accurate geo-coded locations of coal mines in China (Sheng *et al* 2019), known to better than 20 km, spatially finer than the model resolution. Most previous inverse analyses for China used the EDGAR v4.2 or EDGAR v4.3.2 gridded inventories (Janssens-Maenhout *et al* 2019) as their prior estimates for anthropogenic emissions. However, incorrect source locations for coal mining, oil, and natural gas sectors have been found in the EDGAR inventories, which can bias inversion results and lead to erroneous source attribution in top-down estimates (Maasakkers *et al* 2016, Sheng *et al* 2018, 2019, Scarpelli *et al* 2020). For other anthropogenic source sectors we use the EDGAR v4.3.2 as our prior estimates because spatial errors in other source sectors in EDGAR are much smaller than the fossil fuel sector (Maasakkers *et al* 2016). Freshwater aquaculture is mainly co-located with and/or converted from rice growing regions and has been found to be a potential increasing source of methane in China (Yuan *et al* 2019). This source is overlooked in EDGAR v4.3, and thus here we assume that rice growing regions informed by EDGAR v4.3 also include aquaculture. The improved inventory information in our inversion allows us to more accurately quantify emissions and attribute contributions from different source sectors. Uncertainties in source attribution due to prior fractional information are assessed by an ensemble of 1000 inversions using perturbations of the prior inventories (referred to as $SENS_{Prior}$, see section 2 for details). The ensemble uncertainty analysis here is critical to assess sensitivity to different prior estimates and avoid potentially biased interpretation of inversion results. The details of the prior inventories are summarized in table S1 in supplementary information (SI) (available online at stacks.iop.org/ERL/16/104018/mmedia). Throughout this text, our posterior estimates are presented as the mean of the '$SENS_{Prior}$' ensemble with uncertainties represented by $\pm 1\sigma$ of the ensemble. We will also present our EDGAR-based (EDGAR v4.2 as prior) inversions later in the text to demonstrate that trend inference in previous studies for China could have been biased by incorrect emission patterns for coal mining.

2. Methods

2.1. Observations

We use the version 7.2 proxy nadir retrievals of GOSAT methane column data from the University of Leicester (Parker *et al* 2015) in our inverse analysis. GOSAT retrieves the atmospheric methane column by nadir measurements of solar backscatter (1.65 μm absorption band) (Kuze *et al* 2016). Observations are made at three circular pixels of 10 km diameter across the orbit track 260 km apart, separated by 260 km along the track. The same locations are sampled every three days. In China, GOSAT retrieves about 1000 observations per month, but there are more data in the west because of less cloud cover. The number of GOSAT retrievals over a given location does not vary significantly year-to-year and is similar for different seasons, though it is slightly larger during October–December in China (see figure S8 in SI). The ability of GOSAT to constrain regional methane emissions has been shown by previous high resolution

inverse studies for India, Brazil, North America, North Africa, etc (Ganesan *et al* 2017, Tunnicliffe *et al* 2020, Maasakkers *et al* 2021, Western *et al* 2021).

We also include ground-based hourly measurements at (43.2°N, 145.5°E, 96 m above sea level) and Hateruma (24.1°N, 123.8°E, 46.5 m above sea level) stations in Japan operated by the Institute for Environmental Studies (NIES), which have been described in detail by Tohjima *et al* (2014). The two stations are relatively insensitive to China's emissions, but help to improve the constraints to boundary conditions.

2.2. Inversion framework

We use the UK Met Office NAME (Numerical Atmospheric dispersion Modelling Environment) model, a Lagrangian particle dispersion model (Manning *et al* 2011), as the atmospheric transport model used to provide the relationship between emissions and concentrations in the atmosphere. The model domain is 54°E–170°W, 5°S–84°N. We derive an optimized estimate of spatially resolved methane emissions in China using Bayesian inverse analysis. The inversion minimizes the cost function $J(\mathbf{x})$ by solving $\nabla_{\mathbf{x}} J(\mathbf{x}) = 0$, with $J(\mathbf{x})$ defined as follows:

$$J(\mathbf{x}) = \frac{1}{2}(\mathbf{x}-\mathbf{x}_{\text{prior}})^T\mathbf{P}^{-1}(\mathbf{x}-\mathbf{x}_{\text{prior}}) + \frac{1}{2}(\mathbf{y}-\mathbf{H}\mathbf{x})^T\mathbf{R}^{-1}(\mathbf{y}-\mathbf{H}\mathbf{x}). \quad (1)$$

Here $\mathbf{y}$ is the vector of observations, $\mathbf{H}$ is the Jacobian matrix representing the sensitivities of observations to changes in the state vector $\mathbf{x}$ and $\mathbf{x}_{\text{prior}}$ is the the prior value of $\mathbf{x}$. $\mathbf{P}$ is the prior error covariance matrix and $\mathbf{R}$ is the observational error covariance matrix.

The state vector contains 250 elements for aggregated methane emissions per month (200 elements for China) within the model domain using a Gaussian Mixture Model (GMM) with radial basis functions based on spatial proximity and source type patterns (Turner and Jacob 2015). The resulting clustering is shown in figure S10 in SI. The use of the GMM enables us to retain high resolution for major sources up to native model resolution while coarsening resolution for weak or broadly distributed sources. The choice of the number of emission elements in China is based on the suggestions from Turner and Jacob (2015) that balance the aggregation and smoothing errors. The state vector also includes additional four elements for monthly boundary concentrations at the four edges of the model domain to reduce the influence of potential biases in boundary conditions on our derived fluxes (Lunt *et al* 2016, Tunnicliffe *et al* 2020) and one element for an offset parameter between satellite and surface data. The prior boundary concentrations at the domain edges for the Lagrangian particle dispersion model are from a GEOS-Chem 4° × 5° global simulation using methane emissions optimized with GOSAT satellite data Maasakkers *et al* (2019). Here our prior bottom-up inventory is not pre-optimized by the global inversion. The offset parameter (20 ppb *a priori*) accounts for any systematic differences between the GOSAT and the NIES ground-based measurements and their representations by the model Tunnicliffe *et al* (2020). Furthermore, we note that our inversion results are not significantly affected by changing the numbers of emission elements for China (within Turner *et al* suggested range) and the elements for the boundary concentrations (see figure S3 and S10 for in SI for details). We assume 100% prior error for each emission state vector element without correlation (i.e. off-diagonal elements in $\mathbf{P}$ are zero), 2% prior error for boundary conditions, and 50% prior error for the offset parameter. Previous studies (Maasakkers *et al* 2016, Bloom *et al* 2017, Zhang *et al* 2020) have suggested that error correlation is mainly related to natural wetlands (i.e. there are no large error correlations in anthropogenic emissions), while wetland emissions account for less than 5% of China's total emissions and are a minor source in our inversion. We also note that adding small error correlations (5%–20%) for emissions in $\mathbf{P}$ do not change our results (see figure S13 in the SI). Therefore taking a diagonal prior covariance matrix here is appropriate. Observational errors include GOSAT instrument, model transport, and representation errors. We use 10 ppb as the mean observational error (model error + instrument error) standard deviation derived by previous NAME inverse modeling against ground-based observations (Manning *et al* 2011). The GOSAT mean instrument error standard deviation is 11 ppb (Parker *et al* 2015), indicating that satellite instrument error dominates the observational error. For a given satellite observation, we take the maximum of the reported GOSAT instrument error and NAME model error as the observational error added in quadrature to the observational error covariance matrix.

The sensitivity matrix $\mathbf{H}$ is computed by NAME. We release particles at a rate of 2000 particles per hour for each GOSAT retrieval vertical level, over a one minute period centered around the retrieval time, and trace them back in time for 30 d, as done by previous studies (Ganesan *et al* 2017, Tunnicliffe *et al* 2020). For surface sites, we release 20 000 particles at the release height of the stations (100 m and 50 m above sea level for Cape Ochiishi and Hateruma, respectively). Particles are lost when they reach the surface or the four edges of the model domain. The sensitivity matrix $\mathbf{H}$ changes over time depending on different measurement locations and varying meteorology. The OH impact on regional inversions here is negligible. The majority of the sensitivity of a measurement to the surrounding emissions is within 100 km of the measurement location. This implies that air masses will typically travel for a few hours to a few days in this high sensitivity region, during which time and only 0.006%–0.2% of the methane (particles) will be lost due to reaction with OH. The model is

driven by the Unified Model's Model meteorology (Walters *et al* 2014) with horizontal resolution spanning from $0.352° \times 0.234°$ to $0.141° \times 0.094°$ over 2010-2017. The model output is set to be $0.352° \times 0.234°$ for the inversion to be consistent with the lowest meteorological resolution used. NAME has been used extensively to calculate sensitivity matrices for inverses analyses of long-lived greenhouse gases and ozone-depleting gases (Manning *et al* 2011, Ganesan *et al* 2014, 2017, Rigby *et al* 2019, Tunnicliffe *et al* 2020).

We perform the inversion at monthly resolution. We optimize the logarithms of the emission to ensure positivity in all grid cells. Inversions under normal and lognormal assumptions for emissions are previously found to be consistent (Maasakkers *et al* 2019). We found our inversion results between the two assumptions using our baseline prior inventory differ less than 0.6% on sectoral and national scales. Under the lognormal assumption, the inverse problem is non-linear and can be solved numerically by the Levenberg-Marquardt iterative algorithm (Maasakkers *et al* 2019) with a convergence tolerance of 0.05% for maximum relative error:

$$\mathbf{x}_{n+1} = \mathbf{x}_n + (\mathbf{R}^{-1} + \mathbf{H}_n^T\mathbf{P}^{-1}\mathbf{H}_n)^{-1}(\mathbf{H}_n^T\mathbf{P}^{-1}\mathbf{H}_n)^{-1} \times (y - \mathbf{H}\mathbf{x}_n) + \mathbf{R}^{-1}(\mathbf{x}_n - \mathbf{x}_{\text{prior}}) \quad (2)$$

where $\mathbf{H}_n = \partial\mathbf{y}/\partial(\ln\mathbf{x})$ is the Jacobian matrix at the nth iteration. Each individual element $\partial y_i/\partial \ln x_j$ of $\mathbf{H}_n$ can be recalculated in the iteration by $\partial y_i/\partial \ln x_j = x_j\partial y_i/\partial x_j$ with $\partial y_i/\partial x_j$ being individual elements of $\mathbf{H}$ for linear problems computed by the forward model. Validation of inversion results with observations is presented in figures S1 and S2 in SI.

2.3. Sensitivity tests

To test the inversion sensitivity to the prior boundary conditions, we performed 100 inversions by randomly perturbing the boundary conditions on each grid cell at four domain edges (referred to as 'SENS_{BC}'). The perturbations followed a uniform distribution within $\pm 2\%$. We find that 95% (i.e. 2σ) of the ensemble 'SENS_{BC}' results differ less than 0.8% for the national totals and 0.5%–2% for different source sectors (see figure S3). We also performed a sensitivity test on the model XCO_2 by using a different GOSAT proxy product from the RemoTeC v2.3.9, which used the CarbonTracker Model to model XCO_2 (Schepers *et al* 2012), while the University of Leicester GOSAT proxy product used in our inversion is based on an ensemble of model XCO_2 data (Parker *et al* 2015) (figure S4). These sensitivity tests show that inversion results are generally insensitive to different GOSAT proxy product and random perturbations on prior boundary conditions.

To evaluate the inversion sensitivity to the prior fractional information, we perform an ensemble of inversions using 1000 different prior estimates generated by perturbing the baseline prior. This ensemble is referred to as '$\text{SENS}_{\text{Prior}}$' and throughout the text the ensemble mean represents our posterior estimates. For each ensemble member, the relative fraction of a given source sector is perturbed in each grid cell. This is done by randomly selecting a source from coal, rice/aquaculture, livestock, waste, oil/gas, wetlands, or other sectors within the given grid cell and then increasing or decreasing the selected sector emissions following a uniform distribution ($\pm 20\%$). This procedure will also change the total emissions in each grid cell and thus the total emissions for each ensemble member. We neglect grid cells that have small emissions less than 0.5 ton CH_4 per day. We do not perturb source sectors that have a fraction of 0 or 1 in a grid cell (i.e. have no source emissions or dominate the grid cell completely). Overall there are approximately 1500 gridded emissions in China that are perturbed. An example of perturbed sector fractions for the gridded emission inventory is shown in figure S9(a) in SI. We note that the effect of doing the emission perturbation on state vector elements instead of gridded emissions is small (as shown in figure S9 in SI). We prefer to do emission perturbation on the prior $0.352° \times 0.234°$ gridded inventory because it is independent of choice of state vector. This ensemble sensitivity test allows us to assess the effect on source attribution due to uncertainties in relative sector fractions within grid cells (in particular those that have mixed sources). Perturbed sector fractions at grid levels could change the patterns of state vector elements determined by the Gaussian mixture model we used, but we find this change is minimal to our inversion results (see figure S10 in SI).

We also perform two additional inversions using the EDGAR v4.2 inventory and a scaled EDGAR v4.2 inventory as the prior. The latter scales coal mining emissions in EDGAR v4.2 from 28 Tg CH_4 yr^{-1} to 16.7 Tg CH_4 yr^{-1} to match the total emissions of coal mining in the China-specific coal inventory (Sheng *et al* 2019). The purpose of these additional inversions is to demonstrate that large spatial errors in coal mining can lead to biased interpretation of inversion results for China as we discussed in the main text.

3. Results and discussion

3.1. China's national emission estimates and trends

We estimate China's mean annual total methane emissions over 2010–2017 to be 57.6 ± 2.4 Tg CH_4 yr^{-1} (of which 55.2 ± 2.3 Tg CH_4 yr^{-1} are anthropogenic emissions) (figure 1). Our posterior anthropogenic estimates are consistent with the China's 2014 UNFCCC report (UNFCCC 2020) (55.3 ± 2.9 Tg CH_4 yr^{-1}) and with the previous top-down estimates over similar time periods (Maasakkers *et al* 2019, Miller *et al* 2019, Wang *et al* 2019, 2021). The year-to-year variability of our

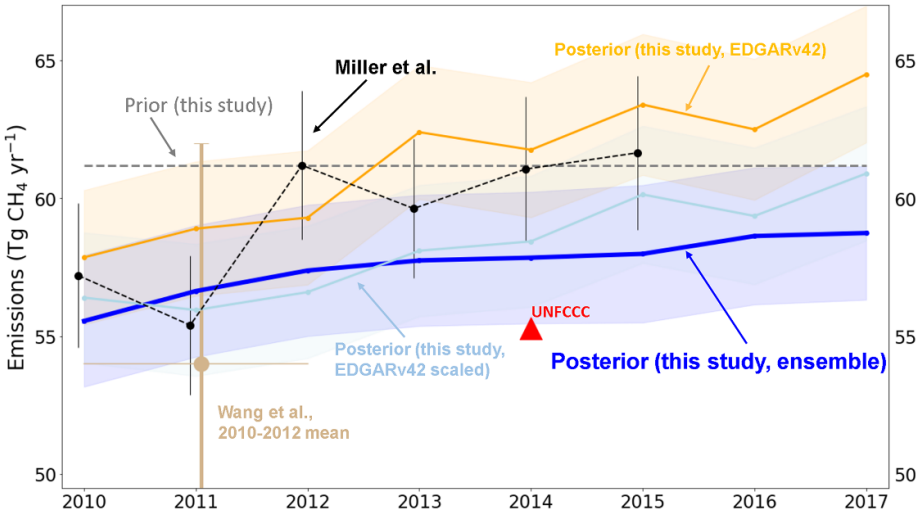

Figure 1. China's national methane emissions over 2010–2017. The posterior estimate from this study (blue) is the mean of the inversion ensemble ($SENS_{Prior}$) with shading corresponding to (1σ) of the ensemble. Two additional inversions using the EDGAR v4.2 (orange) and scaled EDGAR v4.2 (light blue) inventories as the prior are also shown. Bottom-up estimates from China's 2014 UNFCCC report (UNFCCC 2020), and previous top-down estimates with (1σ) uncertainties from Miller *et al* (2019) to Wang *et al* (2019) are provided.

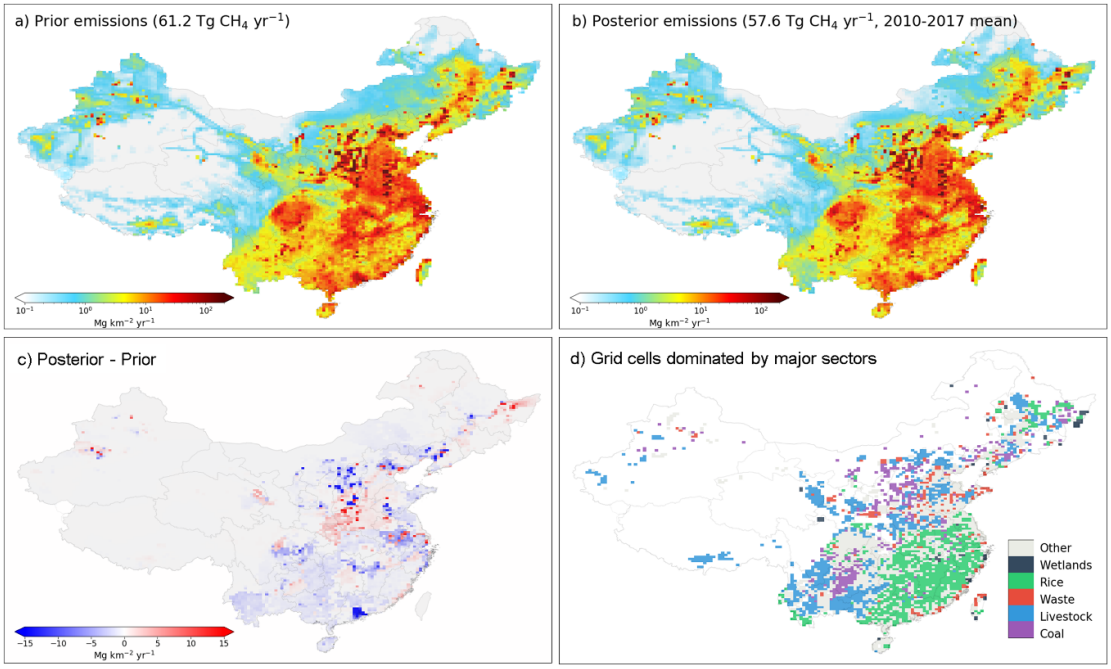

Figure 2. Spatial distribution of China's methane emissions. (a) Prior methane emissions in China from inventories; (b) Mean posterior emissions for 2010–2017 from this study; (c) Absolute difference between mean 2010–2017 posterior emissions and the prior; and (d) Major source sectors for grid cells with high emissions (>5 metric ton per day) and dominated (>50%) by a single source as identified by the prior. 'Other' denotes high emitting grid cells but with no source comprising >50% of a grid cell.

posterior emission estimates is smaller than that found by Wang *et al* (2021). This difference could be attributed to the fact that Wang *et al* refer to an East Asia region that includes many other countries outside of China. In particular, these non-China regions contain wetlands, which are one of the major drivers for year-to-year variability. While our posterior estimates are only 6% lower than the prior (61.2 Tg CH_4 yr^{-1}, figure 1), there are large positive and negative absolute differences on a sub-national/provincial scale that tend to cancel each other on the national scale (figure 2(c)). The relative differences are up to 50% across the country and significant error reductions are mostly over large source regions (see figure S11 in SI).

We find that China's emissions exhibit a statistically significant positive linear trend (0.36 ± 0.04 Tg CH_4 yr^{-2}) for 2010–2017. This trend was slowing down at a statistically significant rate of -0.1 ± 0.04 Tg CH_4 yr^{-3} indicated by the negative coefficient for the

third term in a Legendre polynomial regression (see SI for details). During 2010–2012 China's emissions increase at a rate of 0.77 ±0.2 Tg CH_4 yr^{-2}), then slow after 2012 to 0.3 ± 0.1 Tg CH_4 yr^{-2} for 2012–2017. Our trend estimate for 2010–2015 (0.5 ± 0.2 Tg CH_4 yr^{-2}) is smaller than 1.1 ± 0.4 Tg CH_4 yr^{-2} suggested by a previous study (Miller *et al* 2019) for the same time period. This is discussed further below.

3.2. Emissions and their trends for major source sectors

Fractions of each source in the prior emission inventories can be used to apportion emissions and emission trends to source sectors in countries such as China where the different sources have distinct spatial or temporal distributions (Sheng *et al* 2018, Tunnicliffe *et al* 2020). Coal mining, rice/aquaculture, livestock, and waste are dominant sources for China's anthropogenic emissions. CMM emissions are mainly in Shanxi province and Southwest China, whereas emissions from rice/aquaculture dominate in Southeast China, comparable to the spatial distribution of rice paddies retrieved from the MODIS satellite data (Zhang *et al* 2020). Livestock emissions are mainly concentrated in a number of provinces in north-central and Southwest China, which is consistent with major livestock provinces reported in China Statistical Yearbook (National Bureau of Statistics of China 2020). Waste emissions are localized in urban areas, correlated with population. Wetland emissions are small in China and only dominate a few places in Southeast China and North China. Emissions from other anthropogenic sources and natural sources are too small to dominate any grid cells. Regions having mixed sources (i.e. no source comprising >50% of a grid cell) are mainly in Sichuan and Shandong provinces. Overall, the locations dominated by these major source sectors are well separated at the 0.352° × 0.234° model spatial resolution and account for 70% of the total emissions from China (figure 2(d)).

Coal mining is the largest contributor to the total methane emissions in China with mean 2010–2017 emissions of 14.5 ± 1.4 Tg CH_4 yr^{-1} (table S1). The second largest source in China is rice-aquaculture with mean emissions of 13.2 ± 1.0 Tg CH_4 yr^{-1}, followed by livestock at 11.2 ± 1.1 Tg CH_4 yr^{-1} and waste at 10.2 ± 0.8 Tg CH_4 yr^{-1} (table S1). Trends for these sectors are discussed below, with other minor source sectors showing no significant trends (see figure S5 in SI).

CMM emissions increased by 0.7 ± 0.3 Tg CH_4 yr^{-2} from 2010 to 2012, driving the national trend, but flattened afterwards with a smaller growth of 0.1 ± 0.06 Tg CH_4 yr^{-2} for 2012–2017 (figure 3(a)). According to activity data, coal production peaked in 2013, and in 2016/2017 returned to levels similar to those of 2010 (National Bureau of Statistics of China 2020) (figure 3(b)). The derived emission trend is consistent with coal production activities for 2010–2012 (figure 3(b)), but deviates after that. This inconsistency between top-down estimates and production may be due to emissions from abandoned coal mines. Since 2010/2011, China has consolidated its coal industry to concentrate production in the existing larger and more efficient coal mines (typically state-run mines), and to gradually close a large number of small, village or town-owned coal mines (Zhu *et al* 2017, Sheng *et al* 2019) that are widely spread across the all coal mining fields in China (figure S12 in SI). Our CMM prior inventory includes 11 000 operating coal mines in 2010/2011, of which about 4000 mines have been closed and abandoned over 2010–2017 (Sheng *et al* 2019) (figure 3(b)) but are still allocated in the prior inventory for the inversions. Therefore the derived trend over coal mine fields comprises the contributions from abandoned mines since 2011. An actively venting abandoned mine can emit methane up to 40%–90% of its initial rate in the first 3–4 years, shrinking to 10% after 30 years (US EPA 2004). Increasing emission factors for active coal mines may also explain the inconsistency, but reported recovery rates of CMM have been increasing (Zhu *et al* 2017, Sheng *et al* 2019, Gao *et al* 2020). Thus emission factors are more likely to have decreased or remained stable, which would suggest about 1.7 Tg CH_4 yr^{-1} coming from abandoned coal mines in 2017 assuming emissions in 2017 from active coal mining are similar to those in 2010.

Our CMM emission trend differs from that derived in the previous inverse analysis (Miller *et al* 2019), which uses the EDGAR v4.2 as their prior and shows a continuous increase after 2012 1.0 ± 0.3 Tg CH_4 yr^{-2} (figure 3(a)). We propose that this difference is due to two factors related to the spatial pattern of emissions in the prior. First, the trend in total emissions is higher after 2013. When we use the EDGAR v4.2 as the prior in our inversion rather than the China-specific coal inventory (Sheng *et al* 2019), we derive a similar larger trend after 2012 in the total emissions (figures 1). The magnitude of prior CMM emissions do not significantly influence the posterior trend as indicated by our inversion results using scaled-down EDGAR v4.2 coal emissions (figure 1). This finding indicates that inaccuracies in the spatial distribution of the coal sector in EDGAR can to some extent lead to errors in the derived trend in total emissions. Second, the EDGAR v4.2 inventory at coarse resolution (2° × 2.5°) that were used by the previous global inversion (Miller *et al* 2019) (figure S6 in SI), show that grid cells dominated by coal or mixed sources account for about 85% of the total emissions, in contrast to the high-resolution China-specific inventory used here which has 28% of total emissions from coal dominated grid cells. The strongly differing emission patterns between the two

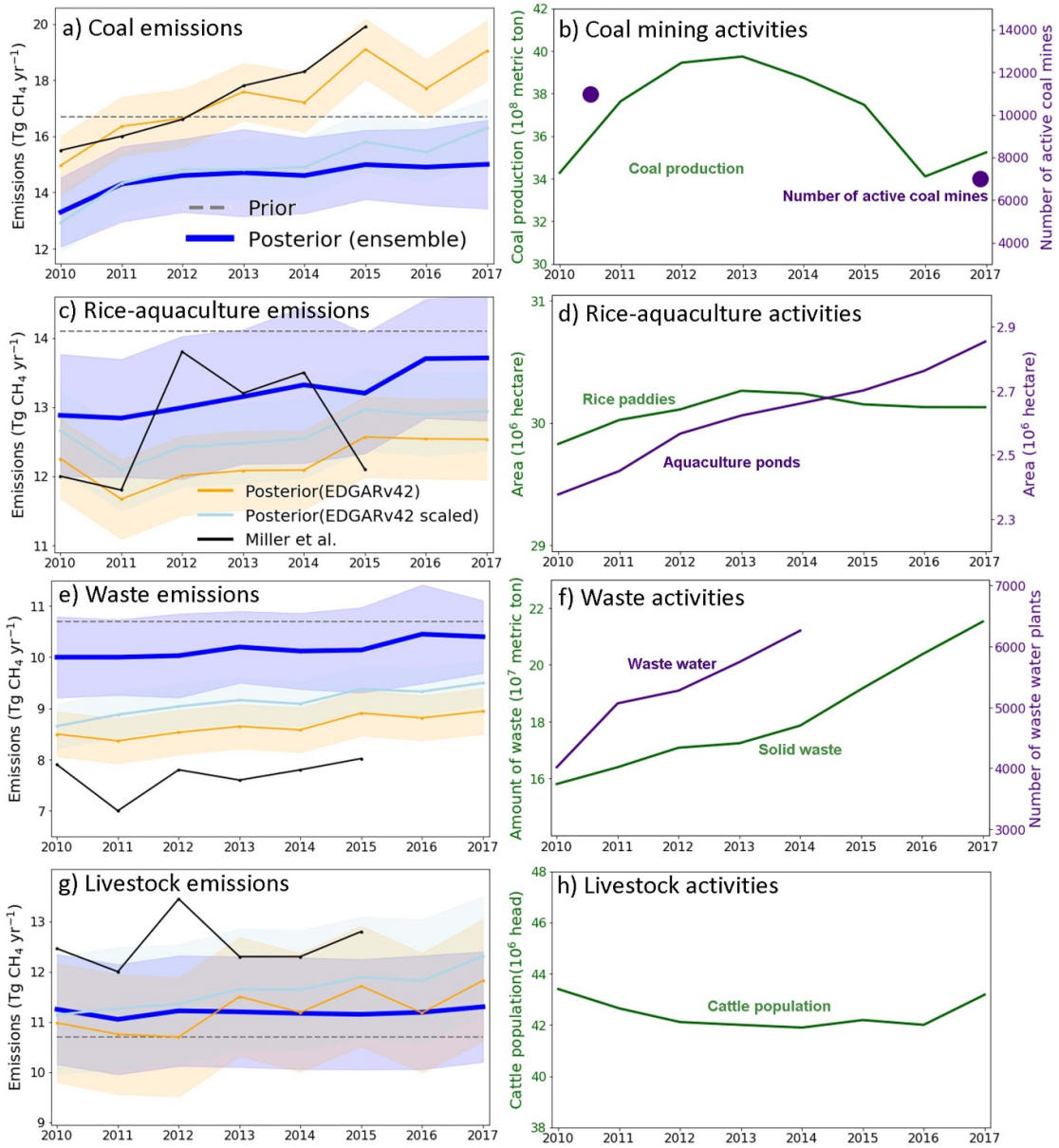

Figure 3. China's methane emissions and emitting activities since 2010 for four major source sectors. (a) and (b) coal methane emissions and mining activities (production and number of active mines); (c) and (d) rice-aquaculture methane emissions and activities (areas for rice paddies and aquaculture ponds); (e) and (f) waste methane emissions and activities (the amount of solid waste at landfills and the number of waste water treatment plants); (g) and (h) livestock methane emissions and activities (cattle population). Shaded areas denote $\pm 1\sigma$ uncertainties from the posterior ensemble ('$SENS_{prior}$'). Our inversion results using EDGAR v4.2 as the prior are also shown in addition to previous results from Miller *et al* (2019). Freshwater aquaculture areas are from Bureau of Fisheries - Ministry of Agriculture, China (2018). Activity data for waste water treatment plants are from Zhao *et al* (2019). Other activity data are from National Bureau of Statistics of China (2020).

inventories remain even at higher spatial resolution (figure S7 in SI). This would lead to a higher apportionment of the total trend to the CMM sector and consequently affect the trends of other source sectors (figures 3(c), (e), (g)). These two factors together may explain the larger derived trend in CMM emissions in the previous work, compared to our estimates.

The emission estimates from rice-aquaculture have increased by 0.13 ± 0.05 Tg CH_4 yr^{-2} from 2010 to 2017. Rice emissions are proportional to paddy area (Eggleston *et al* 2006), but the trend in derived emissions is opposite to that of reported paddy area after 2013 (2% decline from 2013 to 2017 (National Bureau of Statistics of China 2020)). The decline of rice paddy areas is largely related to ongoing conversion of paddy fields towards industrial-scale aquaculture (Yuan *et al* 2019). Freshwater aquaculture in China has emission factors about four times larger than rice cultivation and is estimated to emit 3.5 Tg CH_4 yr^{-1} based on the total area of aquaculture ponds (Yuan *et al* 2019), but has been overlooked in previous gridded bottom-up inventories (such as EDGAR v4.3) and inverse analyses. The freshwater aquaculture industry is primarily located in the southeast of China (figure S12 in SI) (Wang *et al* 2020), where the majority of rice is

grown, and more than half of aquaculture facilities been converted from rice paddies (Yuan *et al* 2019). Therefore the estimated emissions from rice-growing regions informed by the prior include contributions from rice paddies, aquaculture ponds converted from rice paddies, and to a large extent existing aquaculture ponds. China's total area of freshwater aquaculture ponds has increased more than 20% from 2010 to 2017 (National Bureau of Statistics of China 2020) (figure 3(d)). This could explain the opposite trends between emissions and rice paddy areas.

Waste emissions inferred by the inversion exhibit a positive trend of 0.06 ± 0.04 Tg CH_4 yr^{-2} between 2010 and 2017 (figure 3(e)). Landfill methane emissions are partly related to the amount and type of solid waste and management at landfills (Cai *et al* 2018). Due to increased urbanization, the amount to solid waste added per year in China has increased by 50% from 2010 to 2017, and its trend accelerates after 2014 (National Bureau of Statistics of China 2020) (figure 3(f)). In addition, the number of wastewater facilities has increased by 40% from 2010 to 2014 based on the most recent available data (Zhao *et al* 2019) (figure 3(f)), which is potentially a significant source contributing to the waste trend. However we are not able to distinguish contributions from landfills and wastewater because they are both in urban areas and largely co-located at ∼30 km spatial resolution. Waste emissions are also reversely related to local management practices (e.g. recovery rate of waste methane for power generation). This could explain that waste emissions for 2010–2017 do not increase as fast as the amount of waste and the number of facilities.

China's livestock emissions do not exhibit a significant trend (0.01 ± 0.03 Tg CH_4 yr^{-2}) over 2010–2017 (figure 3(g)). Livestock emissions include enteric fermentation and manure management. The former accounts for more than 90% of China's total livestock emissions and is linearly correlated to cattle population, which does not show a significant trend over 2010–2017 but suggests a small decrease between 2010 and 2012 (figure 3(h)). The emission trend from livestock is expected to remain stable in the future because the growing meat consumption in China is due to be met by increasing imports (National Bureau of Statistics of China 2020).

4. Conclusions

Effective climate policies aimed at limiting these emissions will rely on accurate estimates and robust source attribution. In conclusion, our inverse analysis suggests that China's annual methane emissions continue to increase from 2010 to 2017 but we find that the rate of increase has slowed to 0.3 ±0.1 Tg CH_4 yr^{-2} for 2012–2017, as compared to 0.77 ± 0.2 Tg CH_4 yr^{-2} from 2010–2012. We show that emissions from China's coal mining and rice-growing regions have remained positive after 2012 despite a decrease in coal production and in the area harvested for rice. We propose that this may be due to sources such as fugitive emissions from abandoned coal mines and the growth in aquaculture systems in previous rice-growing areas. These sources have not been widely considered in previous national-scale studies of emissions from China. However, our work suggests that they should be carefully considered in any future emission mitigation efforts, as they may have had, and will likely continue to have, a substantial influence on China's overall methane emissions trends. Future measurements of isotopes of atmospheric CH_4 in China should provide improved constraints on source attribution (Rigby *et al* 2012).

Data availability statement

The data that support the findings of this study are openly available at the following URL/DOI: https://catalogue.ceda.ac.uk/uuid/18ef8247f52a4cb6a14013f8235cc1eb.

Acknowledgments

This work was supported by NASA Grant NNX16AC98G to the Massachusetts Institute of Technology. The authors thank Michael B. McElroy, J. William Munger, and Chris Nielsen for helpful discussions. The authors also thank Yasunori Tohjima for providing the data at Cape Ochiishi and Hateruma. Part of this research was carried out at the Jet Propulsion Laboratory, California Institute of Technology, under a contract with the National Aeronautics and Space Administration. RT was funded by the Newton Fund through the Met Office Climate Science for Service Partnership Brazil (CSSP Brazil) and through UK Natural Environment Reseach Council (NERC) grant NE/N016548/1. ALG was funded by NERC Independent Research Fellowship NE/L010992/1. RJP and HB are funded via the UK National Centre for Earth Observation (NE/R016518/1 and NE/N018079/1). Y. Zhang acknowledges funding from NSFC (Project 42007198) and Westlake University. We thank the Japanese Aerospace Exploration Agency, National Institute for Environmental Studies, and the Ministry of Environment for the GOSAT data and their continuous support as part of the Joint Research Agreement. This research used the ALICE High Performance Computing Facility at the University of Leicester for the GOSAT retrievals.

ORCID iDs

Jianxiong Sheng https://orcid.org/0000-0002-8008-3883
Lu Shen https://orcid.org/0000-0003-2787-7016

Tia Scarpelli https://orcid.org/0000-0001-5544-8732
Robert J Parker https://orcid.org/0000-0002-0801-0831
Xin Lan https://orcid.org/0000-0001-6327-6950
Bo Zhang https://orcid.org/0000-0002-5783-6138
Xi Lu https://orcid.org/0000-0002-5063-3776

References

Bergamaschi P *et al* 2013 Atmospheric CH4 in the first decade of the 21st century: Inverse modeling analysis using SCIAMACHY satellite retrievals and NOAA surface measurements *J. Geophys. Res. Atmos.* **118** 7350–69

Bloom A A, Bowman K W, Lee M, Turner A J, Schroeder R, Worden J R, Weidner R, McDonald K C and Jacob D J 2017 A global wetland methane emissions and uncertainty dataset for atmospheric chemical transport models (WetCHARTs version 1.0) *Geosci. Model Dev.* **10** 2141–56

Bureau of Fisheries - Ministry of Agriculture, China 2018 *China Fishery Statistics Yearbooks (2011-2017)* (Beijing: China Agriculture Express)

Cai B, Lou Z, Wang J, Geng Y, Sarkis J, Liu J and Gao Q 2018 CH4 mitigation potentials from China landfills and related environmental co-benefits *Sci. Adv.* **4** eaar8400

Chen H *et al* 2013 Methane emissions from rice paddies natural wetlands, lakes in China: synthesis new estimate *Glob. Change Biol.* **19** 19–32

Dlugokencky E J *et al* 2009 Observational constraints on recent increases in the atmospheric CH_4 burden *Geophys. Res. Lett.* **36** L18803

Eggleston H S, Buendia L, Miwa K, Ngara T and Tanabe K 2006 2006 IPCC guidelines for national greenhouse gas inventories (available at: www.osti.gov/etdeweb/biblio/20880391)

Ganesan A L *et al* 2014 Characterization of uncertainties in atmospheric trace gas inversions using hierarchical Bayesian methods *Atmos. Chem. Phys.* **14** 3855–64

Ganesan A L *et al* 2017 Atmospheric observations show accurate reporting and little growth in India's methane emissions *Nat. Commun.* **8** 836

Ganesan A L *et al* 2019 Advancing scientific understanding of the global methane budget in support of the paris agreement *Glob. Biogeochem. Cycles* **33** 1475–512

Gao J, Guan C and Zhang B 2020 China's CH_4 emissions from coal mining: a review of current bottom-up inventories *Sci. Total Environ.* **725** 138295

Helmig D *et al* 2016 Reversal of global atmospheric ethane and propane trends largely due to US oil and natural gas production *Nat. Geosci.* **9** 490–5 advance online publication

Janssens-Maenhout G *et al* 2019 EDGAR v4.3.2 Global Atlas of the three major greenhouse gas emissions for the period 1970–2012 *Earth Syst. Sci. Data* **11** 959–1002

Kuze A, Suto H, Shiomi K, Kawakami S, Tanaka M, Ueda Y and Buijs H L 2016 Update on GOSAT TANSO-FTS performance, operations and data products after more than 6 years in space *Atmos. Meas. Tech.* **9** 2445–61

Lunt M F, Rigby M, Ganesan A L and Manning A J 2016 Estimation of trace gas fluxes with objectively determined basis functions using reversible-jump Markov chain Monte Carlo *Geosci. Model Dev.* **9** 3213–29

Maasakkers J D *et al* 2016 Gridded national inventory of US methane emissions *Environ. Sci. Technol.* **50** 13123–33

Maasakkers J D *et al* 2019 Global distribution of methane emissions, emission trends and OH concentrations and trends inferred from an inversion of GOSAT satellite data for 2010–2015 *Atmos. Chem. Phys.* **19** 7859–81

Maasakkers J D *et al* 2021 2010-2015 North American methane emissions, sectoral contributions and trends: a high-resolution inversion of GOSAT observations of atmospheric methane *Atmos.Chem. Phys.* **21** 4339–56

Manning A J, O'Doherty S, Jones A R, Simmonds P G and Derwent R G 2011 Estimating UK methane and nitrous oxide emissions from 1990 to 2007 using an inversion modeling approach *J. Geophys. Res.: Atmos.* **116** D2

Miller S M, Michalak A M, Detmers R G, Hasekamp O P, Bruhwiler L M P and Schwietzke S 2019 China's coal mine methane regulations have not curbed growing emissions *Nat. Commun.* **10** 303

Myhre G, Shindell D, Bréon F-M, Collins W, Fuglestvedt J and Huang J 2014 Anthropogenic and natural radiative forcing *Climate Change 2013 — The Physical Science Basis* (Cambridge: Cambridge University Press) 659–740

National Bureau of Statistics of China 2020 China statistical yearbook 2019 *Tech. Rep.* (China Statistics Press)

Nisbet E G *et al* 2019 Very strong atmospheric methane growth in the 4 years 2014–2017: implications for the Paris agreement *Glob. Biogeochem. Cycles* **33** 318–42

Parker R J *et al* 2015 Assessing 5 years of GOSAT Proxy XCH_4 data and associated uncertainties *Atmos. Meas. Tech.* **8** 4785–801

Peng S *et al* 2016 Inventory of anthropogenic methane emissions in mainland China from 1980 to 2010 *Atmos. Chem. Phys.* **16** 14545–62

Rigby M, Manning A J and Prinn R G 2012 The value of high-frequency, high-precision methane isotopologue measurements for source and sink estimation *J. Geophys. Res.: Atmos.* **117** D12

Rigby M, Montzka S A, Prinn R G, White J W C, Young D, O'Doherty S and Park S 2017 Role of atmospheric oxidation in recent methane growth *PNAS* **114** 5373–7

Rigby M, Park S, Saito T, Western L M, Redington A L, Fang X and Young D 2019 Increase in CFC-11 emissions from eastern China based on atmospheric observations *Nature* **569** 546–50

Rigby M, Prinn R G, Fraser P J, Simmonds P G, Langenfelds R L, Huang J and Porter L W 2008 Renewed growth of atmospheric methane *Geophys. Res. Lett.* **35** L22805

Saunois M, Stavert A R, Poulter B, Bousquet P, Canadell J G, Jackson R B and Zhuang Q 2020 The global methane budget 2000–2017 *Earth Syst. Sci. Data* **12** 1561–623

Scarpelli T R, Jacob D J, Maasakkers J D, Sulprizio M P, Sheng J-X, Rose K, Romeo L, Worden J R and Janssens-Maenhout G 2020 A global gridded ($0.1° \times 0.1°$) inventory of methane emissions from oil, gas and coal exploitation based on national reports to the United Nations Framework Convention on Climate Change *Earth Syst. Sci. Data* **12** 563–75

Schaefer H *et al* 2016 A 21st-century shift from fossil-fuel to biogenic methane emissions indicated by $13CH_4$ *Science* **352** 80–4

Schepers D *et al* 2012 Methane retrievals from greenhouse gases observing satellite (GOSAT) shortwave infrared measurements: performance comparison of proxy and physics retrieval algorithms *J. Geophys. Res.* **117** D10307

Sheng J-X, Jacob D J, Turner A J, Maasakkers J D, Sulprizio M P, Bloom A A, Andrews A E and Wunch D 2018 High-resolution inversion of methane emissions in the Southeast US using SEAC4RS aircraft observations of atmospheric methane: anthropogenic and wetland sources *Atmos. Chem. Phys.* **18** 6483–91

Sheng J-X, Song S, Zhang Y, Prinn R G and Janssens-Maenhout G 2019 Bottom-up estimates of coal mine methane emissions in China: a gridded inventory, emission factors and trends *Environ. Sci. Technol. Lett.* **6** 473–8

Thompson R L *et al* 2015 Methane emissions in East Asia for 2000–2011 estimated using an atmospheric Bayesian inversion *J. Geophys. Res.: Atmos.* **120** 4352–69

Tohjima Y *et al* 2014 Temporal changes in the emissions of CH_4 and CO from China estimated from CH_4/CO_2 and CO/CO_2 correlations observed at Hateruma Island *Atmos. Chem. Phys.* **14** 1663–77

Tunnicliffe R L *et al* 2020 Quantifying sources of Brazil's CH_4 emissions between 2010 and 2018 from satellite data *Atmos. Chem. Phys. Discuss.* 1–40

Turner A J, Frankenberg C and Kort E A 2019 Interpreting contemporary trends in atmospheric methane *PNAS* **116** 2805–13

Turner A J, Frankenberg C, Wennberg P O and Jacob D J 2017 Ambiguity in the causes for decadal trends in atmospheric methane and hydroxyl *PNAS* **114** 5367–72

Turner A J and Jacob D J 2015 Balancing aggregation and smoothing errors in inverse models *Atmos. Chem. Phys.* **15** 7039–48

UNFCCC 2020 *Greenhouse Gas Inventory Data Interface* (available at: http://di.unfccc.int/detailed_data_by_party)

US EPA 2004 *Methane Emissions from Abandoned Coal Mines in the United States: Emission Inventory Methodology and 1990-2002 Emissions Estimates* 90 (available at: www.epa.gov/sites/production/files/2016-03/documents/amm_final_report.pdf)

Walters D N *et al* 2014 The met office unified model global atmosphere 4.0 and JULES global land 4.0 configurations *Geosci. Model Dev.* **7** 361–86

Wang F *et al* 2019 Methane emission estimates by the global high-resolution inverse model using national inventories *Remote Sens.* **11** 2489

Wang F *et al* 2021 Interannual variability on methane emissions in monsoon Asia derived from GOSAT and surface observations *Environ. Res. Lett.* **16** 024040

Wang J, Beusen A H W, Liu X and Bouwman A F 2020 Aquaculture production is a large, spatially concentrated source of nutrients in Chinese freshwater and coastal seas *Environ. Sci. Technol.* **54** 1464–74

Western L M, Ramsden A E, Ganesan A L, Boesch H, Parker R J, Scarpelli T R, Tunnicliffe R L and Rigby M 2021 Estimates of North African methane emissions from 2010 to 2017 using GOSAT observations *Environ. Sci. Technol. Lett.* **8** 626–32

Worden J R, Bloom A A, Pandey S, Jiang Z, Worden H M, Walker T W, Houweling S and Röckmann T 2017 Reduced biomass burning emissions reconcile conflicting estimates of the post-2006 atmospheric methane budget *Nat. Commun.* **8** 2227

Yuan J, Xiang J, Liu D, Kang H, He T, Kim S, Lin Y, Freeman C and Ding W 2019 Rapid growth in greenhouse gas emissions from the adoption of industrial-scale aquaculture *Nat. Clim. Change* **9** 318–22

Zhang G, Xiao X, Dong J, Xin F, Zhang Y, Qin Y, Doughty R B and Moore B 2020 Fingerprint of rice paddies in spatial–temporal dynamics of atmospheric methane concentration in monsoon Asia *Nat. Commun.* **11** 1–11

Zhang Y *et al* 2020 Attribution of the accelerating increase in atmospheric methane during 2010–2018 by inverse analysis of GOSAT observations *Atmos. Chem. Phys. Discuss.* 1–42

Zhao X *et al* 2019 China's urban methane emissions from municipal wastewater treatment plant *Earth's Future* **7** 480–90

Zhao Y *et al* 2020 Influences of hydroxyl radicals (OH) on top-down estimates of the global and regional methane budgets *Atmos. Chem. Phys.* **20** 9525–46

Zhu T, Bian W, Zhang S, Di P and Nie B 2017 An improved approach to estimate methane emissions from coal mining in China *Environ. Sci. Technol.* **51** 12072–80